Taylor & Francis
Taylor & Francis Group

ORIGINAL ARTICLE

Check for updates

Micromechanical fiber-matrix interface model for in-plane shear in unidirectional laminae

Lucas L. Vignoli[a] (iD), Marcelo A. Savi[b] (iD), Pedro M. C. L. Pacheco[c] (iD), and Alexander L. Kalamkarov[d] (iD)

[a]Center for Technology and Applications of Composite Materials, Department of Mechanical Engineering, Universidade Federal do Rio de Janeiro, Macaé, Brazil; [b]Center for Nonlinear Mechanics, COPPE – Department of Mechanical Engineering Universidade Federal do Rio de Janeiro, Rio de Janeiro, Brazil; [c]Department of Mechanical Engineering, Centro Federal de Educação Tecnológica Celso Suckow da Fonseca CEFET/RJ, Rio de Janeiro, Brazil; [d]Department of Mechanical Engineering, Dalhousie University, Halifax, Canada

ABSTRACT

A novel analytical model is proposed for the in-plane shear response of unidirectional composites on account of fiber-matrix interface. The fiber-matrix interface influences the stiffness and induces nonlinear phenomena, playing a fundamental role in the damage onset and propagation. The interface consists of three zones: fiber-transition, core, and matrix-transition. The transition zones are assumed to have zero thicknesses, while the core zone is a layer with finite thickness. Fiber-transition zone is characterized by a nonlinear damage behavior. The analytical model is verified by comparing with finite element simulations and experimental data, indicating adequate description of the complex phenomena under study.

1. Introduction

The design of composite materials is challenging due to many variables and scales involved [1,2], as well as the stochastic issues related to the manufacturing processes [3]. The World-Wide Failure Exercise summarizes the state of the art of macromechanical studies considering failure criteria [4–6].

Most of the recent advances considering composite nonlinear response are obtained numerically [7–9]. Nevertheless, micromechanical analytical models have the advantage of low computational cost [10], which is useful for multiscale analysis [11] and optimization procedures [12]. One of the major challenges of composite design is to evaluate damage mechanisms [13–15]. Some recent experimental advances are reported considering damage tracking using digital image correlation [16,17] and thermography [18–20].

The micromechanics of composite materials usually estimates the effective elastic properties [21–23] and strengths [24,25] based on the essential assumption of a perfectly brittle failure of the unidirectional composites. On this basis, a linear elastic response is assumed until the rupture. This assumption is too strong for in-plane shear loads [26–28] and therefore, it is important to incorporate the fiber-matrix interface nonlinear behavior to properly describe composite behavior.

Kolanu et al. [29] showed that the composite nonlinear shear behavior may significantly affect the response of notched specimens. Chen et al. [30] pointed out that the

nonlinearity induced by shear also influences the longitudinal compressive failure of unidirectional laminae. These studies highlight the importance to consider the in-plane shear nonlinear response for different applications. Hence, an analytical investigation relating micromechanical interface damage with macromechanical composite nonlinearity considering in-plane shear load is desirable to improve the damage understanding.

Andrianov et al. [31] evaluated the interface between fiber and matrix using the asymptotic homogenization technique. Zhang & Waas [32] and Patel et al. [33] used analytical concentric cylinder model to evaluate interface effects. Würkner et al. [34] assumed that imperfect interface can be modeled as an elastic element. An interesting comparative discussion about different methodologies to evaluate imperfect bonding including interface can be found in Sevostianov et al. [35]. Nevertheless, these approaches are not able to evaluate the mechanism responsible for interface debonding damage, being only able to compute the effective in-plane shear modulus of unidirectional laminae with an interface (perfect or imperfect).

Riaño et al. [36] pointed out that fiber-matrix interface has mechanical properties different from matrix bulk material, which are difficult to be measured or estimated. Subramanian et al. [37] and Koyanagi et al. [38] reported the influence of fiber surface treatment on the interface strength and on the composite failure.

The fiber-matrix interface has a finite dimension, being characterized by a core zone and two transition zones, one
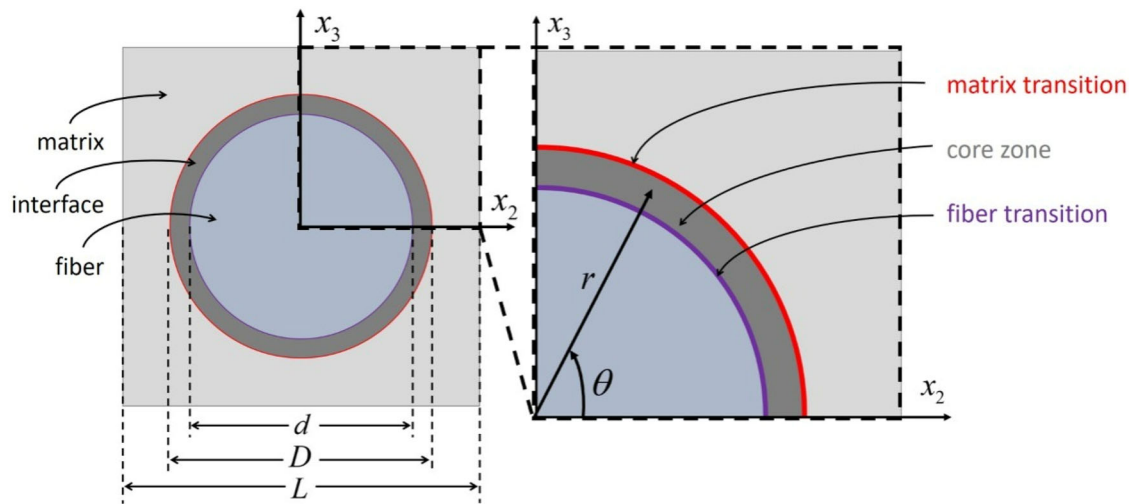
Figure 1. Unit cell with square symmetry showing interface split into three zones: fiber-transition, core and matrix-transition.

close to the fiber (fiber-transition) and the other one close to the matrix (matrix-transition). Literature presents different terms to characterize this interface and sometimes employs interface for the transition zone and interphase for its core region.

The present paper develops an analytical micromechanical model to estimate the in-plane shear behavior of unidirectional laminae taking into account the influence of fiber-matrix interface in the composite nonlinear behavior. A novel model is proposed accounting for the fiber-matrix interface composed by three zones: fiber-transition, core, and matrix-transition. The transition zones are assumed to have zero thicknesses, while the core zone is a layer with finite thickness. Fiber-transition zone is characterized by a nonlinear damage behavior while the matrix-transition is perfectly bonded. This assumption is commonly adopted due to the abrupt variation of mechanical properties [39]. The derivation of the analytical model is presented, being followed by a model based on finite element (FE) method. Verification and discussion are presented in the sequel considering experimental data. Properties estimated by the analytical model are used as an input for the FE simulations, which shows the capabilities of the novel approach. Afterward, a sensitivity analysis is performed to discuss the influence of the parameters introduced in the analytical formulation.

2. Analytical formulation

A novel analytical model to deal with in-plane shear load is proposed based on the VSPKc model developed by Vignoli et al. [23] to estimate the effective elastic properties of unidirectional composites. The novel approach includes a finite dimension interface composed of three zones: core zone and two transition zones, fiber-transition and matrix-transition. The fiber-transition zone is subjected to damage, which significantly affects the composite behavior. On the other hand, matrix-transition zone is perfectly bonded.

Figure 1 shows the unit cell considered for the analytical model. The fiber distribution is assumed with square symmetry, resulting in a square unit cell with length L along the directions x_2 and x_3. Additionally, the fiber has diameter d, interface has a finite dimension in such a way that the transition zones are assumed to be zero-thickness while the core zone has internal and external diameters d and D, respectively. Despite some authors proposed a simplified approach modeling fibers with square [40] and octagonal [41] cross-sections, the fiber geometry has a significant influence on the composite response [42]. Either Cartesian coordinates $x_2 - x_3$ or polar coordinates $r - \theta$ can be used, and the more convenient one is employed for the calculations.

The model is derived in two steps. First, the elastic regime is evaluated, where fiber-transition and matrix-transition zones are assumed to be perfectly bonded. Under this assumption, the elastic response of the composite interface is only related to the core zone, which means that the transition zones do not have any influence. Hammerand et al. [43] pointed out that the solid interface influences the effective elastic properties of the composites. Afterward, the inelastic regime is of concern and the maximum load transferred between fiber and interface is due to interface shear strength, S_s^i.

2.1. Elastic regime – core zone influence

This section discusses a linear elastic composite subjected to in-plane shear considering the interface influence that is due to the core zone. Based on the unit cell presented in Figure 1, the composite volume is given by a sum of fiber, interface and matrix volume fractions, $V_f + V_i + V_m = 1$, where fiber volume fraction is $V_f = \pi d^2/4L^2$ and interface volume fraction is $V_i = \pi(D^2 - d^2)/4L^2$. Therefore, the matrix volume fraction is $V_m = 1 - (\pi D^2/4L^2)$. The following geometrical relations are helpful for the analytical derivation discussed next: $d/L = 2\sqrt{V_f/\pi}$ and $D/L = 2\sqrt{(V_i + V_f)/\pi}$.

By assuming a symmetric unit cell, the analysis can be restricted to $0 \le x_3 \le L/2$. The unit cell is also split into three parts: $0 \le x_3 \le d/2$, part (1); $d/2 < x_3 \le D/2$, part
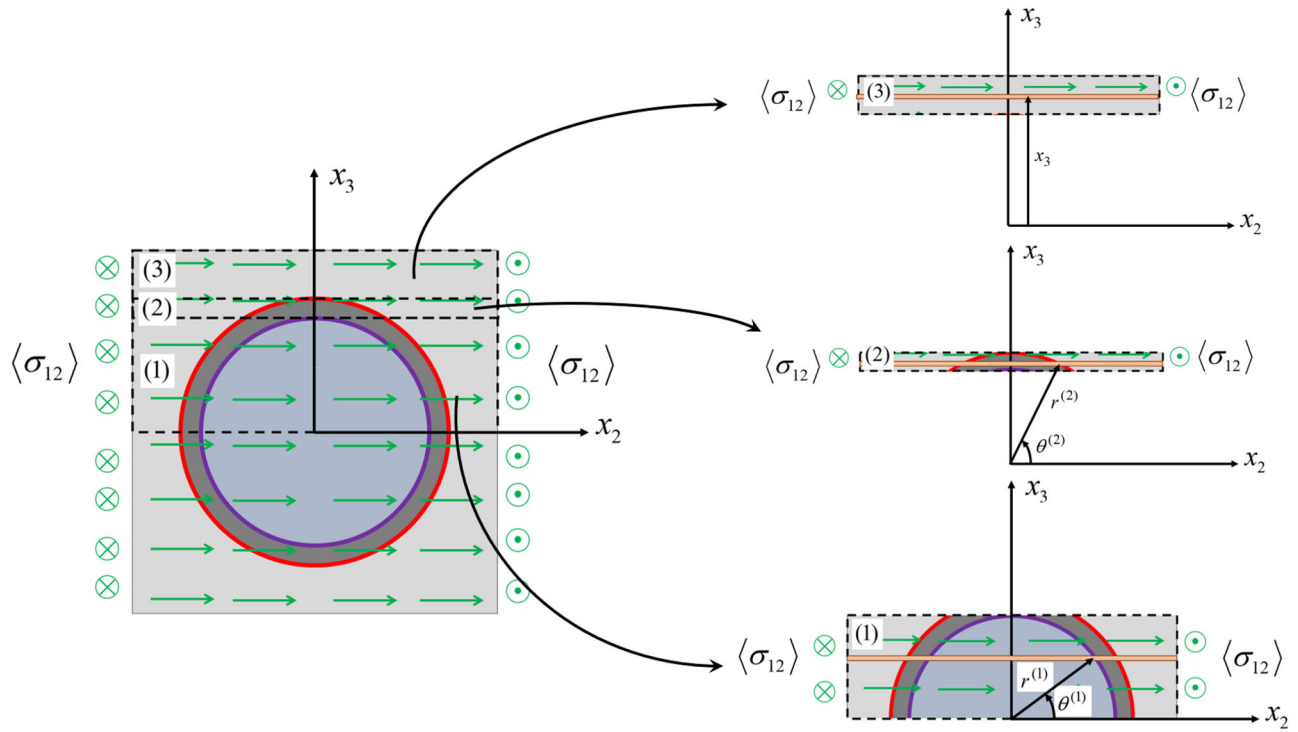
Figure 2. Load distribution on the unit cell and parts (1, 2) and (3); the orange thick lines represent the infinitesimal element in an angles $\theta^{(1)}$ and $\theta^{(2)}$ for parts (1) and (2), respectively, and the vertical position x_3 for part (3).

(2); and $D/2 < x_3 \le L/2$, part (3). Note that, using polar coordinates, $r^{(1)}$ is defined at the interface inner radius (fiber-transition) and $r^{(2)}$ at the interface outer radius (matrix-transition). On this basis, the equilibrium and geometrical compatibility requirements of the unit cell are established, as represented in Figure 2, by the following equations:

$$\langle \sigma_{12} \rangle = \frac{2}{L} \left(\int_0^{d/2} \sigma_{12}^{(1)} dx_3 + \int_{d/2}^{D/2} \sigma_{12}^{(2)} dx_3 + \int_{D/2}^{L/2} \sigma_{12}^{(3)} dx_3 \right) \quad (1)$$

$$\langle \varepsilon_{12} \rangle = \varepsilon_{12}^{(1)} = \varepsilon_{12}^{(2)} = \varepsilon_{12}^{(3)} \quad (2)$$

where the $\langle \sigma_{12} \rangle$ and $\langle \varepsilon_{12} \rangle$ are the effective shear stress and strain on the unit cell, respectively, and $\sigma_{12}^{(1)}$, $\sigma_{12}^{(2)}$, $\sigma_{12}^{(3)}$, $\varepsilon_{12}^{(1)}$, $\varepsilon_{12}^{(2)}$ and $\varepsilon_{12}^{(3)}$ are the shear stresses and strains in parts (1, 2) and (3).

By considering the first integral of Eq. (1), the infinitesimal element showed in Figure 2 for part (1) illustrates that there are three phases in series for this load: fiber, interface and matrix. The transition zones are negligible since it is assumed a perfectly bonded condition and therefore, the interface is represented by the core zone. The equilibrium requirement, the geometrical compatibility and the constitutive elastic relations are expressed by

$$\sigma_{12}^{(1)} = \sigma_{12}^{(1,m)} = \sigma_{12}^{(1,i)} = \sigma_{12}^{(1,f)} \quad (3)$$

$$\varepsilon_{12}^{(1)} = V_f^{(1)} \varepsilon_{12}^{(1,f)} + V_i^{(1)} \varepsilon_{12}^{(1,i)} + V_m^{(1)} \varepsilon_{12}^{(1,m)} \quad (4)$$

$$\sigma_{12}^{(1,f)} = 2G_{12}^f \varepsilon_{12}^{(1,f)} \quad (5)$$

$$\sigma_{12}^{(1,i)} = 2G^i \varepsilon_{12}^{(1,i)} = 2\lambda G^m \varepsilon_{12}^{(1,i)} \quad (6)$$

$$\sigma_{12}^{(1,m)} = 2G^m \varepsilon_{12}^{(1,m)} \quad (7)$$

where $\sigma_{12}^{(1,m)}$, $\sigma_{12}^{(1,i)}$ and $\sigma_{12}^{(1,f)}$ are the shear stresses, $\varepsilon_{12}^{(1,f)}$, $\varepsilon_{12}^{(1,i)}$ and $\varepsilon_{12}^{(1,m)}$ are the shear strains, $V_f^{(1)}$, $V_i^{(1)}$ and $V_m^{(1)}$ are the volume fractions of the phases in an arbitrary infinitesimal element in part (1); G_{12}^f, G^i and G^m are the phase shear moduli. Due to uncertainties about the interface properties, it is usual to assume $G^i = \lambda G^m$ [44], where λ is the ratio of interface and matrix shear moduli. Note that the constituent volume fractions inside part (1) are $V_f^{(1)} = (d/L) \cos \theta^{(1)}$, $V_i^{(1)} = [(D-d)/L] \cos \theta^{(1)}$ and $V_m^{(1)} = 1 - V_f^{(1)} - V_i^{(1)}$; alternatively, it is possible to use the geometrical relations previously defined, $V_f^{(1)} = 2\sqrt{V_f/\pi} \cos \theta^{(1)}$, $V_i^{(1)} = 2[\sqrt{(V_i + V_f)/\pi} - \sqrt{V_f/\pi}] \cos \theta^{(1)}$ and $V_m^{(1)} = 1 - 2\sqrt{(V_i + V_f)/\pi} \cos \theta^{(1)}$.

Manipulating Eq. (3–7), the strain-stress relation of the infinitesimal element is

$$\varepsilon_{12}^{(1)} = \left(\frac{V_f^{(1)} \lambda G^m + V_i^{(1)} G_{12}^f + V_m^{(1)} \lambda G_{12}^f}{\lambda G^m G_{12}^f} \right) \frac{\sigma_{12}^{(1)}}{2} \quad (8)$$

Replacing the volume fractions in Eq. (8), the following equation is obtained

$$\sigma_{12}^{(1)} = 2G^m \left(\frac{1}{1 + a_{12}^{(1)} \cos \theta^{(1)}} \right) \varepsilon_{12}^{(1)} \quad (9)$$

where $a_{12}^{(1)} = 2\{[(1/\lambda) - 1]\sqrt{(V_i + V_f)/\pi} + [(G^m/G_{12}^f) - (1/\lambda)]\sqrt{V_f/\pi}\}$.

On this basis, the effective shear modulus of the arbitrary infinitesimal element of part (1) is the following,

$$G_{12}^{(1)}(\theta^{(1)}) = G^m\left(\frac{1}{1 + a_{12}^{(1)}\cos\theta^{(1)}}\right) \quad (10)$$

Therefore, the first integral of Eq. (1) with $x_3 = (d/2)\sin\theta^{(1)}$ and $dx_3 = (d/2)\cos\theta^{(1)}d\theta^{(1)}$, and considering the compatibility relation in Eq. (2), furnishes

$$\int_0^{d/2}\sigma_{12}^{(1)}dx_3 = \int_0^{d/2}2G_{12}^{(1)}\varepsilon_{12}^{(1)}dx_3$$

$$= 2G^m\langle\varepsilon_{12}\rangle\frac{d}{2}\int_0^{\pi/2}\left(\frac{\cos\theta^{(1)}}{1 + a_{12}^{(1)}\cos\theta^{(1)}}\right)d\theta^{(1)} \quad (11)$$

A symbolic integration is carried out using MATLAB, furnishing the following general form:

$$I(a, \theta) = \int\left(\frac{\cos\theta}{1 + a\cos\theta}\right)d\theta$$

$$= \begin{cases} -\sin\theta + K & \text{if } a = 0 \\ \frac{\theta}{a} - \frac{1}{a\sqrt{a^2-1}}\ln\left(\frac{a + \cos\theta + \sin\theta\sqrt{a^2-1}}{a\cos\theta + 1}\right) + K & \text{otherwise} \end{cases} \quad (12)$$

where K is a generic integral constant. Note that for any a, $I(a, 0) = 0 + K$.

Replacing Eq. (12) into Eq. (11),

$$\int_0^{d/2}\sigma_{12}^{(1)}dx_3 = 2G^m\langle\varepsilon_{12}\rangle\frac{d}{2}\left[I(a_{12}^{(1)}, \pi/2) - I(a_{12}^{(1)}, 0)\right] \quad (13)$$

The second integral of Eq. (1) is now of concern, adopting the same procedure. The equilibrium and compatibility equations are given by

$$\sigma_{12}^{(2)} = \sigma_{12}^{(2,m)} = \sigma_{12}^{(2,i)} \quad (14)$$

$$\varepsilon_{12}^{(2)} = V_f^{(2)}\varepsilon_{12}^{(2,f)} + V_i^{(2)}\varepsilon_{12}^{(2,i)} \quad (15)$$

Since part (2) does not include the fiber, $V_f^{(2)} + V_i^{(2)} = 1$. Additionally, $V_i^{(2)} = (D/L)\cos\theta^{(2)} = 2[\sqrt{(V_i + V_f)/\pi}]\cos\theta^{(2)}$ and $V_m^{(2)} = 1 - V_i^{(2)} = 1 - 2\sqrt{(V_i + V_f)/\pi}\cos\theta^{(2)}$. Manipulating these equations and assuming a linear elastic constitutive relation, the following expression is obtained

$$\sigma_{12}^{(2)} = 2G^m\left(\frac{\lambda}{V_i^{(2)} + \lambda V_m^{(2)}}\right)\varepsilon_{12}^{(2)} \quad (16)$$

Replacing the interface and matrix volume fraction, the effective shear modulus of an infinitesimal element in part (2) is

$$G_{12}^{(2)}(\theta^{(2)}) = G^m\left(\frac{1}{1 + a_{12}^{(2)}\cos\theta^{(2)}}\right) \quad (17)$$

where $a_{12}^{(2)} = 2[(1/\lambda) - 1]\sqrt{(V_i + V_f)/\pi}$.

Using relations between Cartesian and polar coordinates, $x_3 = (D/2)\sin\theta^{(2)}$ and $dx_3 = (D/2)\cos\theta^{(2)}d\theta^{(2)}$, the second integral of Eq. (1) is the following

$$\int_{d/2}^{D/2}\sigma_{12}^{(2)}dx_3 = 2G^m\langle\varepsilon_{12}\rangle\frac{D}{2}\int_{\theta_i}^{\pi/2}\left(\frac{\cos\theta^{(2)}}{1 + a_{12}^{(2)}\cos\theta^{(2)}}\right)d\theta^{(2)} \quad (18)$$

where $\theta_i = a\sin(d/D) = a\sin[\sqrt{V_f/(V_i + V_f)}]$.

Note that the integral in Eq. (18) is equivalent to Eq. (12) and hence,

$$\int_{d/2}^{D/2}\sigma_{12}^{(2)}dx_3 = 2G^m\langle\varepsilon_{12}\rangle\frac{D}{2}\left[I(a_{12}^{(2)}, \pi/2) - I(a_{12}^{(2)}, \theta_i)\right] \quad (19)$$

Finally, part (3) is of concern and, since it is restricted to matrix, the integral is solved directly as follows,

$$\int_{D/2}^{L/2}\sigma_{12}^{(3)}dx_3 = 2G^m\langle\varepsilon_{12}\rangle\left(\frac{L - D}{2}\right) \quad (20)$$

Replacing Eq. (13), (18) and (20) in Eq. (1),

$$\langle\sigma_{12}\rangle = 2G^m\langle\varepsilon_{12}\rangle\left(1 + 2\sqrt{\frac{V_f}{\pi}}\left[I(a_{12}^{(1)}, \pi/2)\right]\right.$$

$$\left. + 2\sqrt{\frac{V_i + V_f}{\pi}}\left[I(a_{12}^{(2)}, \pi/2) - I(a_{12}^{(2)}, \theta_i) - 1\right]\right) \quad (21)$$

By analyzing Eq. (21), the composite in-plane shear modulus is given by

$$G_{12} = G^m\left(1 + 2\sqrt{\frac{V_f}{\pi}}\left[I(a_{12}^{(1)}, \pi/2)\right]\right.$$

$$\left. + 2\sqrt{\frac{V_i + V_f}{\pi}}\left[I(a_{12}^{(2)}, \pi/2) - I(a_{12}^{(2)}, \theta_i) - 1\right]\right) \quad (22)$$

2.2. Damage onset and propagation – fiber-transition zone influence

The damage of unidirectional laminae under in-plane shear is complex since both matrix and interface may be damaged. This investigation assumes that damage occurs in the interface, being restricted to the fiber-transition zone.

By considering the geometrical compatibility presented in Eq. (2), $\langle\varepsilon_{12}\rangle = \varepsilon_{12}^{(1)}$, using the constitutive relations and the definitions of $G_{12}^{(1)}$ presented in Eq. (10), the following expression is reached

$$\sigma_{12}^{(1)} = \frac{G_{12}^{(1)}}{G_{12}}\langle\sigma_{12}\rangle = \left(\frac{1}{1 + a_{12}^{(1)}\cos\theta^{(1)}}\right)\frac{G^m}{G_{12}}\langle\sigma_{12}\rangle \quad (23)$$

The interface damage needs to be evaluated from the shear stresses in polar coordinates. Since the shear stress $\sigma_{12}^{(1)}$ is defined in Cartesian coordinates, the interface shear stresses in polar coordinates are given by

$$\tau_{zr} = \sigma_{12}^{(1)} \cos \theta^{(1)} \tag{24}$$

$$\tau_{z\theta} = -\sigma_{12}^{(1)} \sin \theta^{(1)} \tag{25}$$

where τ_{zr} and $\tau_{z\theta}$ are the shear stresses along the fiber-transition interface.

It is adopted that just the radial component of the shear stress induces damage, $\tau_{zr} = S_s^i$, where S_s^i is the interface shear strength [45,46]. In addition, it is assumed that $\langle \sigma_{12} \rangle = S_{12}^{s,o}$ on the damage onset, where $S_{12}^{s,o}$ is the onset in-plane shear strength. Manipulating Eq. (23) and (24), the composite damage onset is reached when

$$S_{12}^{s,o} = (1 + a_{12}^{(1)}) \frac{G_{12}}{G^m} S_s^i \tag{26}$$

Similar procedure can be applied to evaluate the damage propagation, assuming that the load in part (1) must be separated into two parts: damaged and undamaged zones, as represented in Figure 3. It is noticeable that damage region is defined by a specific value of θ, θ_d that defines the transition between damaged and undamaged interfaces, which is defined by the condition $\tau_{zr}(\theta_d) = S_s^i$.

On this basis, Eq. (1) needs to consider the damaged and undamaged regions, being rewritten as follows

$$\langle \sigma_{12} \rangle = \frac{2}{L} \left(\int_0^{\theta_d} \sigma_{12}^{(1)} \frac{d}{2} \cos \theta^{(1)} d\theta^{(1)} + \int_{\theta_d}^{\pi/2} \frac{d}{2} \sigma_{12}^{(1)} \cos \theta^{(1)} d\theta^{(1)} \right.$$
$$\left. + \int_{d/2}^{D/2} \sigma_{12}^{(2)} dx_3 + \int_{D/2}^{L/2} \sigma_{12}^{(3)} dx_3 \right) \tag{27}$$

A considerable damage propagation occurs before composite rupture, inducing a nonlinear behavior [4–6]. Moreover, according to ASTM D3518M-18, the in-plane shear test must stop when there is a rupture or when if $2\langle \varepsilon_{12} \rangle = 5\%$, indicating that damage is expected to propagate in a stable way up to $\langle \varepsilon_{12} \rangle = 2.5\%$. Hence, a stable propagation can be assumed. Additionally, by hypothesis, it is assumed that the interface force remains constant around the damaged region after damage onset. Based on these assumptions, the first integral of Eq. (27) is

$$\int_0^{\theta_d} \sigma_{12}^{(1)} \frac{d}{2} \cos \theta^{(1)} d\theta^{(1)} = \int_0^{\theta_d} \frac{S_s^i}{\cos \theta^{(1)}} \frac{d}{2} \cos \theta^{(1)} d\theta^{(1)} = S_s^i \frac{d}{2} \theta_d \tag{28}$$

The second integral is similar with the one presented in Eq. (13), just changing the inferior limit,

$$\int_{\theta_d}^{\pi/2} \frac{d}{2} \sigma_{12}^{(1)} \cos \theta^{(1)} d\theta^{(1)} = 2G^m \langle \varepsilon_{12} \rangle \frac{d}{2} \left[I(a_{12}^{(1)}, \pi/2) - I(a_{12}^{(1)}, \theta_d) \right] \tag{29}$$

And the third and fourth integrals of Eq. (27) are the same of those presented in Eqs. (19) and (20). Manipulating these results, the following relation is reached,
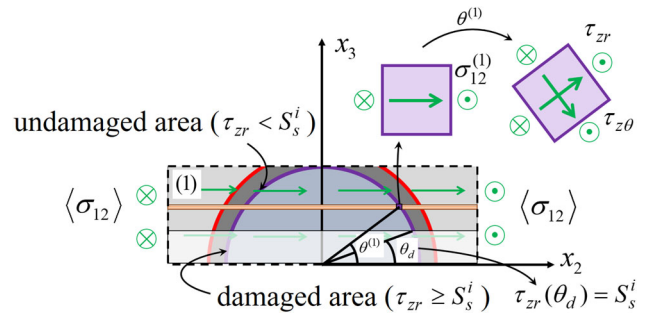

Figure 3. Transition between damaged and undamaged areas defined by $\tau_{zr}(\theta_d) = S_s^i$.

$$\langle \sigma_{12} \rangle = 2 \sqrt{\frac{V_f}{\pi}} \theta_d S_s^i + 2 G_{12}^T \langle \varepsilon_{12} \rangle \tag{30}$$

where G_{12}^T is the lamina in-plane shear tangent modulus defined by

$$G_{12}^T = G^m \left(1 + 2\sqrt{\frac{V_f}{\pi}} \left[I(a_{12}^{(1)}, \pi/2) - I(a_{12}^{(1)}, \theta_d) \right] \right.$$
$$\left. + 2\sqrt{\frac{V_i + V_f}{\pi}} \left[I(a_{12}^{(2)}, \pi/2) - I(a_{12}^{(2)}, \theta_i) - 1 \right] \right) \tag{31}$$

For any damaged angle $0° \leq \theta_d < 90°$, the effective shear strain and stress can be computed by considering that $\tau_{zr}(\theta_d) = S_s^i$ and $\langle \varepsilon_{12} \rangle = \varepsilon_{12}^{(1)}$, obtaining

$$\langle \varepsilon_{12} \rangle = \left(\frac{1 + a_{12}^{(1)} \cos \theta_d}{\cos \theta_d} \right) \frac{S_s^i}{2G^m} \tag{32}$$

Alternatively, for a strain-driven load, the damaged angle for $\langle \varepsilon_{12} \rangle \geq S_{12}^{s,o}/2G_{12}$ is given by

$$\theta_d = a \cos \left(\frac{S_s^i}{2G^m \langle \varepsilon_{12} \rangle - a_{12}^{(1)} S_s^i} \right) \tag{33}$$

3. Finite element model

An FE model is developed to analyze in-plane shear load using the commercial software Ansys 2022 R1. Fiber, matrix and core interface are modeled as linear elastic materials. Fiber is assumed to be transversally isotropic while matrix is isotropic. The interface shear modulus is defined by $G^i = \lambda G^m$ [36, 44]. Interface and matrix are perfectly bonded, while the fiber-transition zone is modeled using cohesive elements that are usually applied for interface failure in micromechanical studies [47–49].

Cohesive elements employ the separation-distance model to evaluate the contact debonding, where perfectly bonded behavior is assumed if the interface shear traction, τ, is smaller than S_s^i and the relation between interface shear traction and the tangential relative displacement, δ, is defined by

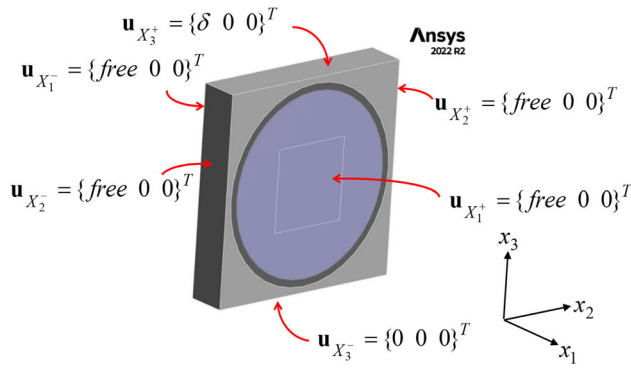$$\tau = \left(1 - \frac{\delta}{\delta_c} \right) S_s^i \tag{34}$$

Figure 4. Boundary conditions of the FE model.

where δ_c is the critical tangential displacement when interface is completely damaged. When $\delta \geq \delta_c$, the interface stiffness is zero. For a detailed discussion about cohesive elements, see Zhang et al. [50] and Fernandes & Campilho [51].

Solid quadratic elements, SOLID186, are employed together with contact pairs, CONTA174 and TARGE170. Displacement-driven simulations are carried out assuming boundary conditions to satisfy the periodicity of the unit cell, as presented in Figure 4 [52]: $\mathbf{u}_{X_1^+} = \mathbf{u}_{X_1^-} = \mathbf{u}_{X_2^+} = \mathbf{u}_{X_2^-} = \{free\ 0\ 0\}^T$, $\mathbf{u}_{X_3^+} = \{\delta\ 0\ 0\}^T$ and $\mathbf{u}_{X_3^-} = \{0\ 0\ 0\}^T$.

4. Verification and Discussion

The verification of the novel analytical model is carried out in two steps. Initially, the model estimations are compared with experimental data, where the interface properties are calibrated (V_i, λ and S_s^i). This first step is fundamental since interface properties cannot be measured directly. Next, the analytical results are compared with the FE simulations. The same calibrated interface properties are used as input to the numerical approach to demonstrate the consistency of mechanical modeling. Analytical results are evaluated considering a strain-driven monotonic load and the shear stress is computed using equations presented in the Section 2. On the other hand, FE simulations adopts a displacement-driven monotonic load where shear strain is computed by geometrical relation and stress is computed by force reaction.

Experimental results are based on Kaddour et al. [53] that considers an IM7 carbon fiber together with an 8552 epoxy matrix. IM7 carbon fiber is transversally isotropic with the following properties: longitudinal elastic modulus $E_1^f = 276GPa$, transversal elastic modulus $E_2^f = 19GPa$, in-plane shear modulus, $G_{12}^f = 27GPa$, out-of-plane shear modulus $G_{23}^f = 7GPa$ and in-plane Poisson's ratio $\nu_{12}^f = 0.2$. The 8552 epoxy matrix is isotropic with shear modulus $G^m = 1.478Pa$ and Poisson's ratio $\nu^m = 0.38$. Based on Riaño et al. [36] and Wang et al. [44], the core interface shear modulus is $G^i = \lambda G^m$ and $\nu^i = \nu^m = 0.38$ [53]. Fiber diameter is $d = 4.5\mu m$, and volume fraction is $V_f = 0.6$.

Matzenmiller & Gerlach [54] highlighted that the interface properties cannot be obtained testing the bulk matrix due to the influence of manufacturing process in composite materials and therefore, an inverse problem is employed. In
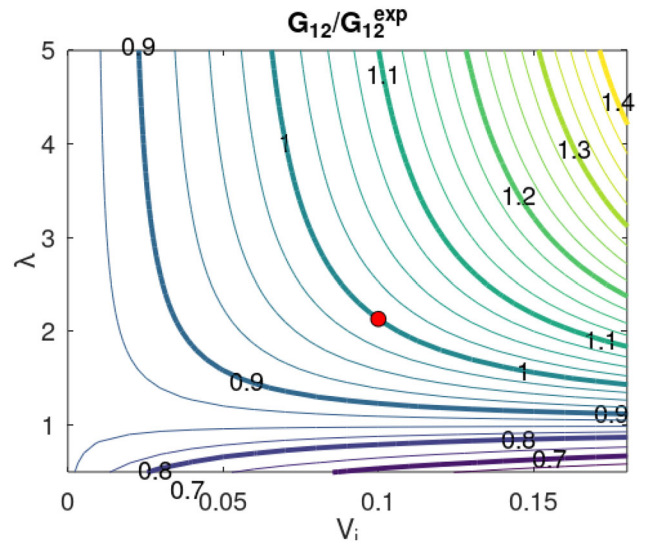

Figure 5. Influence of interface volume fraction, V_i, and the ratio between core interface and matrix shear moduli, λ, on the in-plane shear modulus, G_{12}.
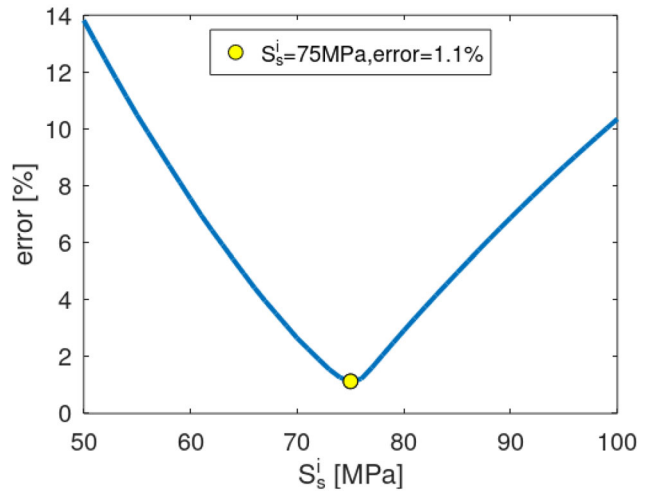

Figure 6. Absolute error on the in-plane shear stress-strain curve according to the interface shear strength, S_s^i.

order to evaluate the influence of interface volume fraction, V_i, and the ratio between core interface and matrix shear moduli, λ, Figure 5 shows the ratio between analytical estimations and experimental value of the in-plane shear modulus, $G_{12}^{exp} = 5.6GPa$, for $0.05 < V_i < 0.18$ and $0.5 < \lambda < 5$. As expected, due to the analytical model consistence, when $V_i = 0$ or $\lambda = 1$ the analytical estimation has the same value: $G_{12}/G_{12}^{exp} = 0.855$. These conditions imply that the interface has zero-thickness when $V_i = 0$ or that the interface has the same properties as the matrix if $\lambda = 1$. These conditions are equivalent to the composite without interface effect and the developed analytical model is equivalent to the proposed by Vignoli et al. [23].

There are many combinations of V_i and λ that result in $G_{12} = G_{12}^{exp}$ for the selected lamina. Maligno et al. [55] reported $0.45 < \lambda < 2.22$ and $V_i = 0.0257$; Chang et al. [56] considered $1 < \lambda < 3$ and $0.04 < V_i < 0.3$; and Wang et al. [57] assumed $1 < \lambda < 6$ and $0.01 < V_i < 0.1$. The best option is to use micrography to measure the interface volume fraction and use the proposed analytical formulation
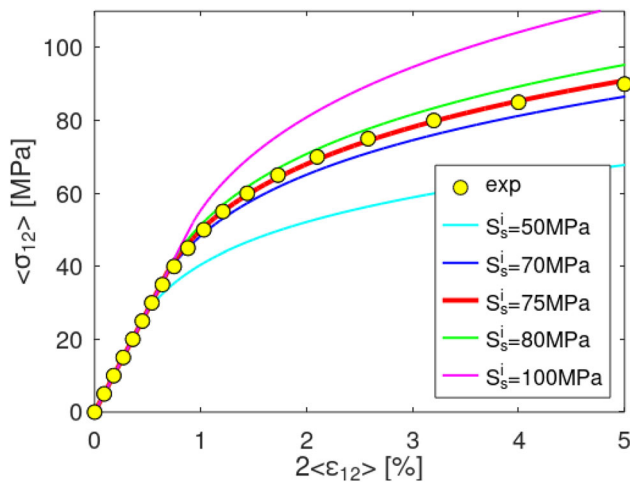
Figure 7. Influence of interface shear strength, S_s^i, on the in-plane shear stress-strain curve; comparison with experimental data from Kaddour et al. [53].

Figure 8. Converged mesh of the FE model.

just to obtain λ. However, the litereture presents very few information about V_i and there is a lack of solid knlowdge about the interface. On this basis, since there is not information related to these parameters, it is adopted $V_i = 0.1$ and $\lambda = 2.134$, a combination represented by the red circle in Figure 5.

The interface influence on the shear strength is evaluated by considering all the points of the experimental in-plane shear stress-strain curve reported by Kaddour et al. [53]. By assuming a strain-driven load, the analytical stresses are compared with the experimental data keeping $V_i = 0.1$ and $\lambda = 2.134$. Figure 6 presents the average absolute error comparing the analytical estimations and the experimental stress data for $50MPa < S_s^i < 100MPa$. The minimum error is 1.1% for $S_s^i = 75MPa$, which can be adopted as a good estimation.

Figure 7 presents a comparison of the in-plane shear stress-strain curves obtained by the proposed analytical model and experimental data from Kaddour *et al.* [53], using $V_i = 0.1$, $\lambda = 2.134$ and the following values for S_s^i: 50, 70, 75, 80, and 100 MPa. Note that S_s^i influences the damage onset and its propagation. Results present a close agreement for $70MPa < S_s^i < 80MPa$, but $S_s^i = 75MPa$ obtained the best fit comparing all the experimental data.

It should be pointed out that the properties V_i, λ and S_s^i must be obtained comparing the analytical estimation with the experimental data. This adjustment cannot be avoided since the interface properties are not measured directly. By assuming $V_i = 0.1$, $\lambda = 2.13$ and $S_s^i = 75MPa$ as input, FE simulations are carried out considering the following values for δ_c: 0.1 μm, 1 μm, 1 mm and 1 m. These simulations aim to show that the proposed analytical model is physically consistent.

A mesh with 31725 elements and 153596 nodes is employed after a convergence analysis, as illustrated in Figure 8. Results are presented in Figure 9, indicating an excellent agreement among the analytical model, FE simulation, and experimental data. For $\delta_c = 0.1\mu m$ there is an abrupt stiffness variation around $2\langle\varepsilon_{12}\rangle = 1.5\%$, indicating an unstable propagation of interface damage. For $\delta_c = 1\mu m$, $\delta_c = 1mm$, and $\delta_c = 1ma$ similar behavior is observed, even with a difference of 10^3 in the critical tangential

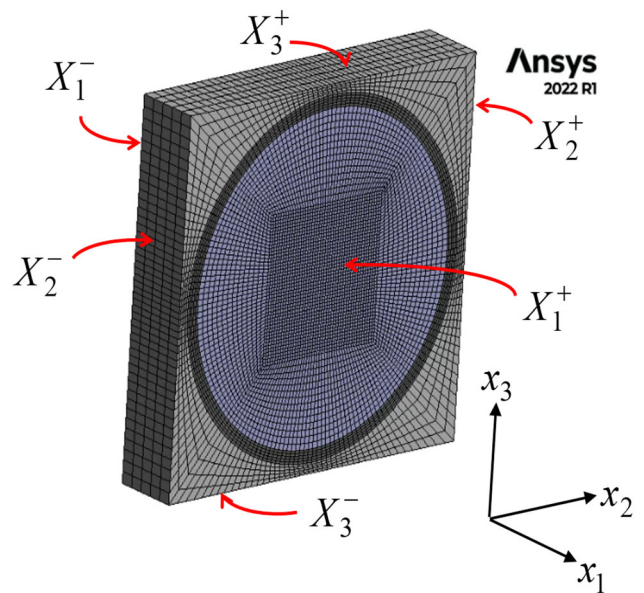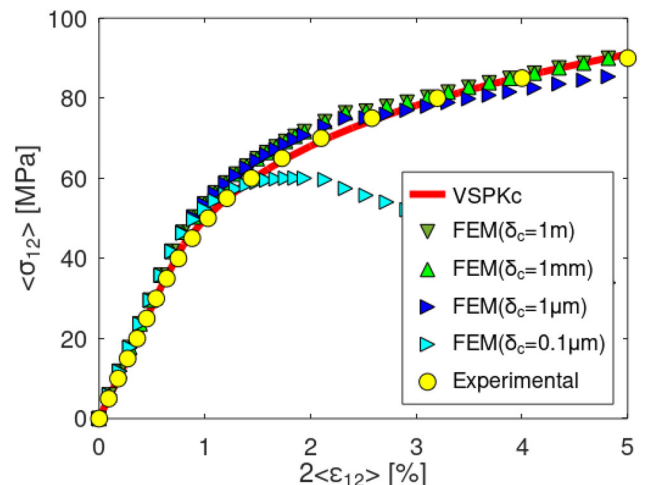**Figure 9.** Comparison between analytical and numerical models with experimental data from Kaddour et al. [53].

displacement, indicating a stable damage propagation up to $2\langle\varepsilon_{12}\rangle = 5\%$, as expected for most composites according to the ASTM D3518M-18 [58]. It is important to highlight that the interface damage is assumed just in the fiber-transition zone in the analytical and FE models. Although it is not assured that the matrix damage or plasticity is absent, results indicate that its effect can be neglected since analytical and numerical results based on this assumption show good agreement with experimental data. It is important to highlight that this simplification, i.e. disregarding the matrix plasticity effect, results in a much simpler modeling approach from the analytical point of view.

Results of the micromechanical in-plane shear stress, σ_{12}, distributions for finite element simulations are presented in Figure 10 for the following strain values $2\langle\varepsilon_{12}\rangle$: 0.1%, 1%, 3%, and 5%. For the finite element model, $\delta_c = 1m$ is considered henceforward, since a stable damage propagation is realized for this parameter and results of Figure 9 indicate that this value reproduces the experimental results. Note
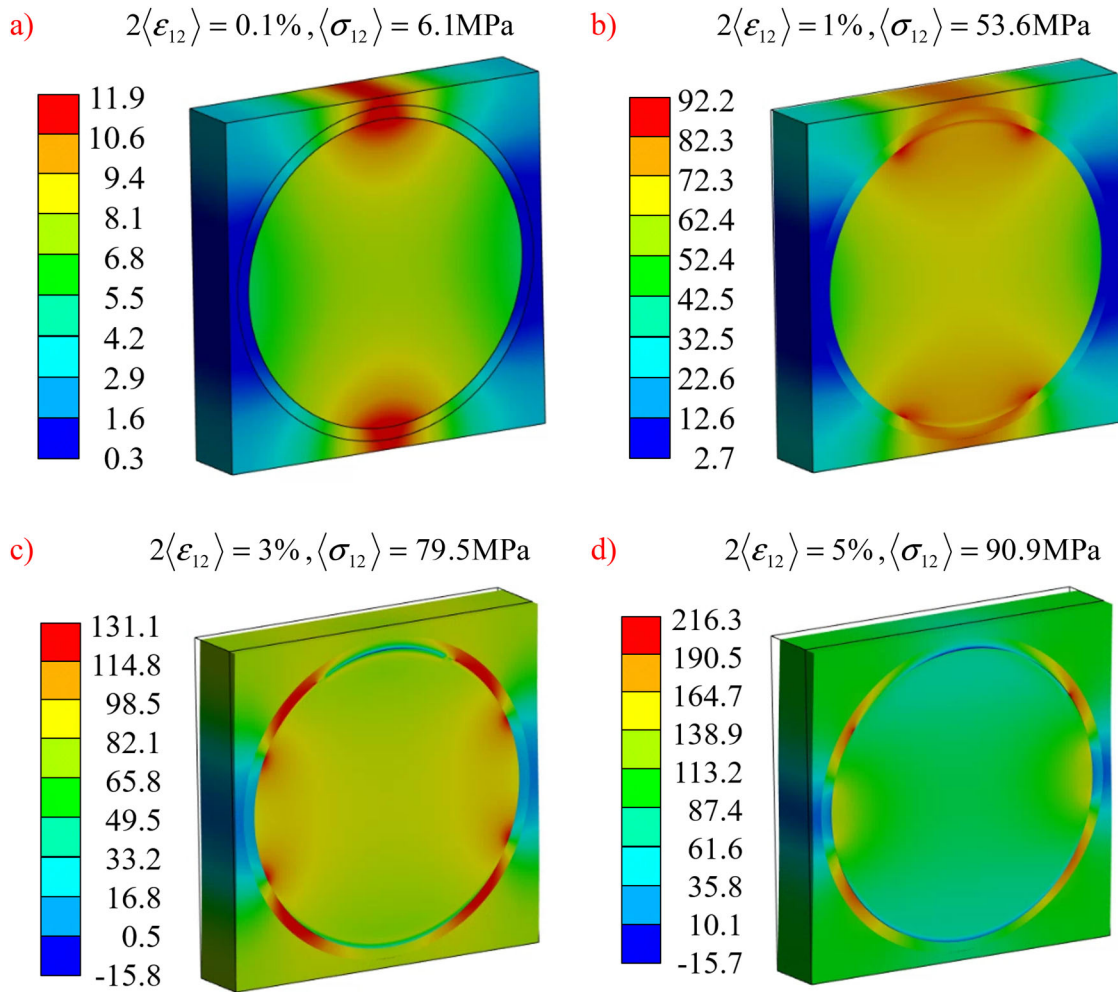
a) $2\langle\varepsilon_{12}\rangle = 0.1\%, \langle\sigma_{12}\rangle = 6.1\mathrm{MPa}$ b) $2\langle\varepsilon_{12}\rangle = 1\%, \langle\sigma_{12}\rangle = 53.6\mathrm{MPa}$

c) $2\langle\varepsilon_{12}\rangle = 3\%, \langle\sigma_{12}\rangle = 79.5\mathrm{MPa}$ d) $2\langle\varepsilon_{12}\rangle = 5\%, \langle\sigma_{12}\rangle = 90.9\mathrm{MPa}$

Figure 10. In-plane shear stress distributions for in-plane shear strains equal to: a) 0.1%; b) 1%; c) 3%; d) 5%.

that the macromechanical shear stress are represented by $\langle\sigma_{12}\rangle$ for each strain level, but the micromechanical stress distribution in nonuniform due to stress concentration inside the unit cell. These results indicate that the micromechanical shear stress levels are higher than usually required for yielding epoxy matrices, in agreement with experimental observations that report matrix micro-cracking during the shear load [13]. Despite that possible inelastic behavior of the matrix, results presented in Figure 9 evidence that it can be disregarded for the sake of simplicity and the effective behavior of the composite can be well reproduced considering the nonlinearity source only from the interface.

Figure 11 shows the distribution of the shear stress, τ_{zr}, which is responsible for interface damage, along the fiber-transition zone. First, for $2\langle\varepsilon_{12}\rangle = 0.1\%$, an undemaged interface is observed and the composite response is in an elastic regime. The analytical computation is close to numerical results, indicating that load distribution assumption is effective. For the other strain levels, $2\langle\varepsilon_{12}\rangle = 1\%$, $2\langle\varepsilon_{12}\rangle = 3\%$, and $2\langle\varepsilon_{12}\rangle = 5\%$, the traction distribution has a similar trend, but the difference between damaged angles from analytical and numerical models increases according to the strain level. Despite this difference, results indicate that $\tau_{zr} = S_s^i = 75MPa$ is constant along the damaged regions and overall, composite response is not sensitive to the

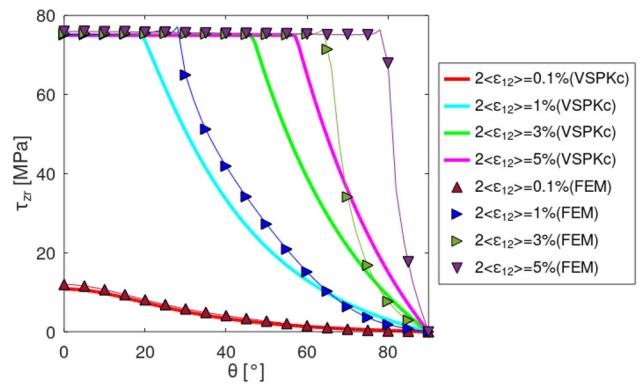**Figure 11.** Comparison between analytical (VSPKc) and numerical (FEM) resultes of the shear traction, τ_{zr}, along the interface for different strain levels.

damaged angle. This conclusion can be understood realizing that the stress tends to be almost constant when the damage propagates for high strain levels, even when the damage angle is increasing.

5. Parametric analysis

Once the proposed modeling is validated against experimental data and numerical simulation, this Section aims to
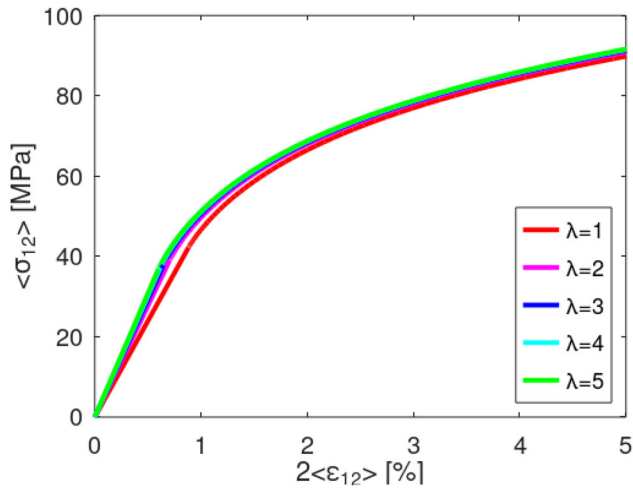
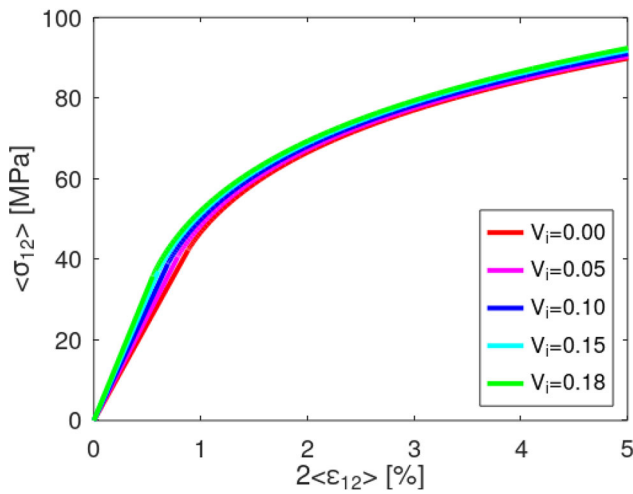**Figure 12.** Influence of $\lambda = G^i/G^m$ on the in-plane shear stress-strain curve.

Figure 13. Influence of V_i on the in-plane shear stress-strain curve.
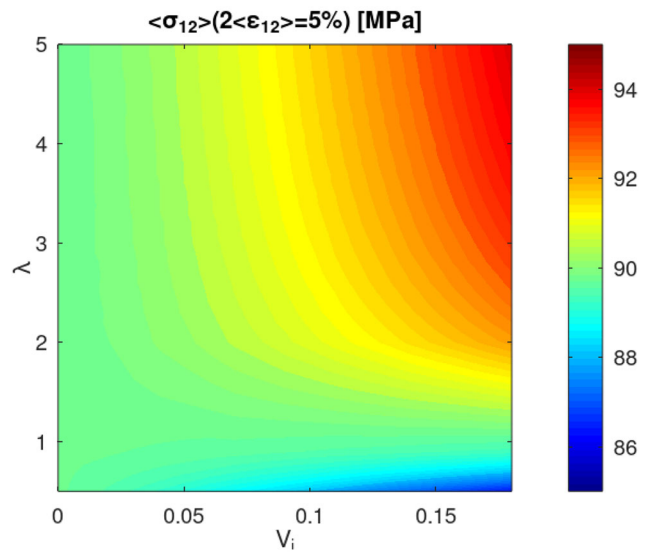

Figure 14. Influence of $\lambda = G^i/G^m$ and V_i on the $\langle \sigma_{12} \rangle$ for $2\langle \varepsilon_{12} \rangle = 5\%$.
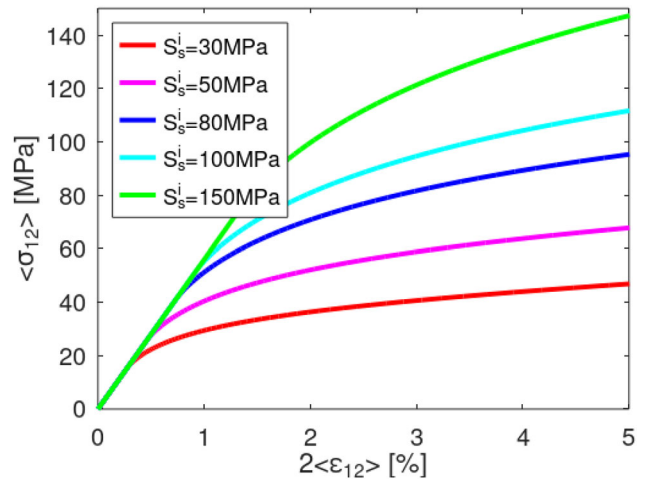

Figure 15. Influence of S_s^i on the in-plane shear stress-strain curve.

present a parametric sensitive analysis relate to parameters that cannot be directly measured by fibers and matrix tests: $\lambda = G^i/G^m$, V_i and S_s^i.

Figure 12 shows the in-plane shear stress-strain curves for $\lambda = 1, 2, 3, 4, 5$ considering the IM7 carbon fiber and 8552 epoxy matrix properties with $V_f = 0.6$, $V_i = 0.1$ and $S_s^i = 75 MPa$. Additionally, results presented in Figure 13 are obtained for $\lambda = 2.134$ and with the following values for V_i: 0.00, 0.05, 0.10, 0.15, and 0.18. These results indicate that the nonlinear behavior has low sensitivity with respect to λ and V_i. Note that the influence of these parameters on the elastic response is already discussed in Figure 5.

Figure 14 allows a more detailed analysis showing the maximum shear stress $\langle \sigma_{12} \rangle$ when $2\langle \varepsilon_{12} \rangle = 5\%$, which is equivalent to the in-plane shear strength according to ASTM D3518M-18 [58]. The experimental strength reported by Kaddour et al. [53] is 90 MPa, which means that the analytical estimations have a good agreement with experimental data.

To evaluate the interface shear strength, $V_i = 0.1$ and $\lambda = 2.134$ are assumed, evaluating results for $S_s^i = 30 MPa$, $50 MPa, 80 MPa, 100 MPa, 150 MPa$. Figure 15 highlights that S_s^i is the most important parameter for the in-plane shear

stress-strain curve since the region with material nonlinear behavior is predominant.

6. An approach to obtain the in-plane shear stress-strain curve

This Section proposes an alternative way to obtain the in-plane shear stress-strain curve using the previously derived analytical formulation. A possible approach can be assume $V_i = 0.1$, computing λ to get an analytical shear modulus expressed by Eq. (22) equal to the experimental values. Nevertheless, based on the parametric analysis discussed in Section 5, λ and V_i do not have great influence for damage onset and propagation, and the unidirectional laminae subjected to in-plane shear have a nonlinear behavior in most part of the stress-strain curve. Therefore, for the sake of simplicity, $\lambda = 2$ and $V_i = 0.1$ are assumed for all results in this Section.

The required inputs of the analytical model are V_f, G^m, G_{12}^f, and S_s^i. Usually, V_f, G^m, and G_{12}^f are available from datasheets or average values can be used from literature.
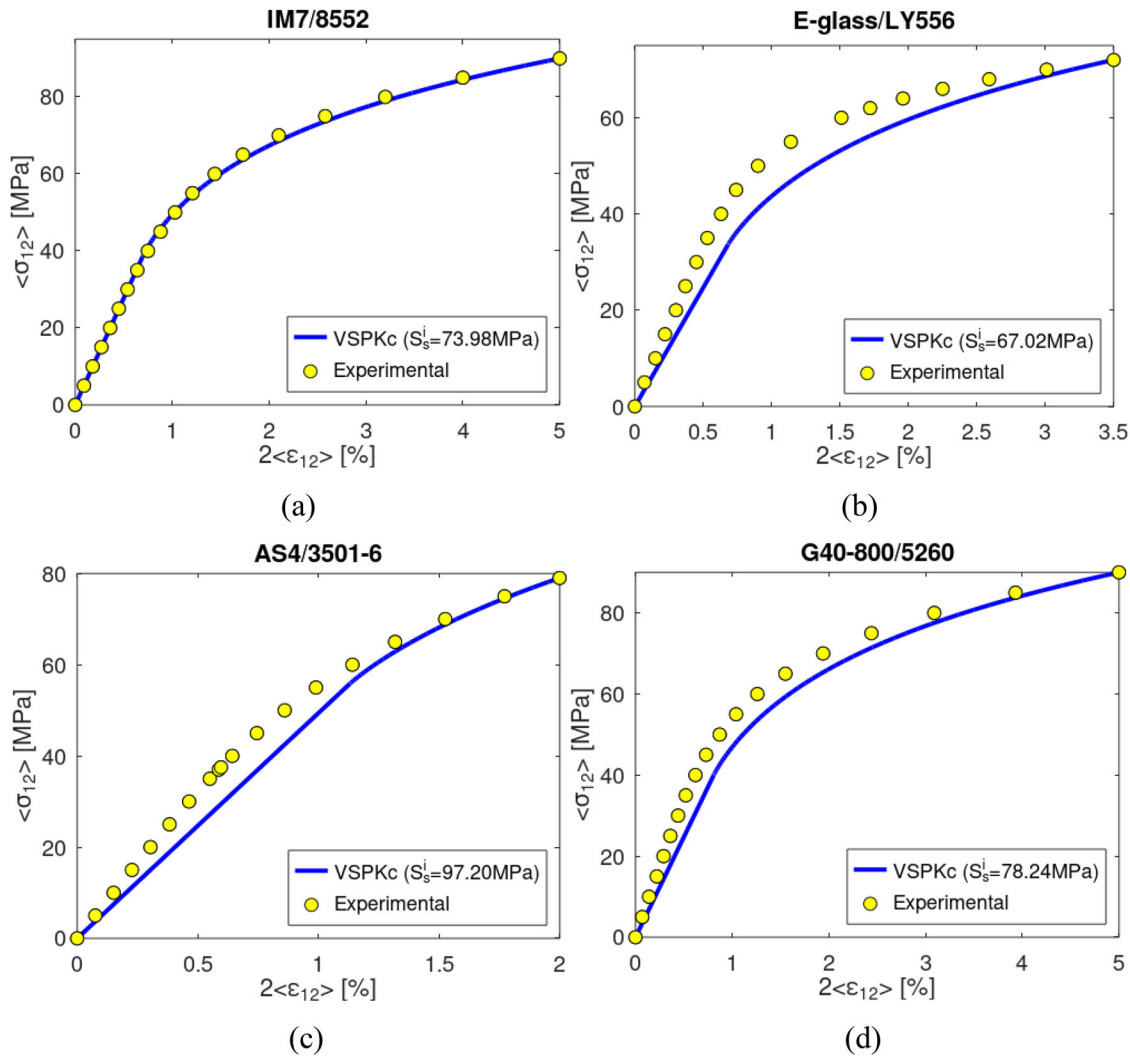
Figure 16. Experimental [53] and VSPKc in-plane shear stress-strain curves assuming $\lambda = 2$ and $V_i = 0.1$: (a) IM7/8552; (b) E-glass/LY556; (c) AS4/3501-6; (d) G40-800/5260.

Alternatively, S_s^i is fitted using the rupture values for $\langle\sigma_{12}\rangle$ and $\langle\varepsilon_{12}\rangle$. To follow the standard recommendation, $\langle\varepsilon_{12}\rangle = 2.5\%$ is selected if the rupture happens when $2\langle\varepsilon_{12}\rangle > 5\%$. In addition, it is important to highlight that S_s^i cannot be obtained experimentally, but from solving an inverse problem.

Figure 16 shows a comparison between experimental and analytical curves for all the laminae from WWFE3 [53]. The interface shear strengths callibrated for IM7/8552, E-glass/LY556, AS4/3501-6, and G40-800/5260 are $S_s^i = 73.98MPa$, $S_s^i = 67.02MPa$, $S_s^i = 97.20MPa$, and $S_s^i = 78.24MPa$, respectively. It is noticeable a good agreement especially for the nonlinear behavior that indicates the damage propagation. Once again, the damage propagation modeling hypothesis seems to be able to reproduce the experimental results, indicating that interface damage is more important than matrix plasticity. Concerning the linear behavior, $\lambda = 2$ and $V_i = 0.1$ are also demonstrated to be good average values to represent unidirectional laminae.

Choi et al. [59] presented a discussion about different experimental tests to evaluate the in-plane shear load. The

authors performed tests with ± 45° layup specimen with tensile load [58], which is the most usual procedure due to its simple apparatus, Iosipescu test [60], and V-notched rail shear tests [61]. A brief overview of the advantages and drawbacks of different test apparatus can be found in ASTM D4762-18 [62]. The focus of the present investigation is not to discuss the experimental issues but it is rather to validate the proposed modeling.

The laminae tested by Choi et al. [59] was made with SKYFLEX-USN-150 carbon fiber and K51 epoxy matrix. Despite that the authors did not precise the constituents' properties, $V_f = 0.6$, $G^m = 1.5GPa$, and $G_{12}^f = 15GPa$ are assumed as typical values for CFRP. Additionally, the point with $2\langle\varepsilon_{12}\rangle = 5\%$ is adopted considering the average between the three experimental methods to obtain the interface shear strengths, despite that the obtained maximum shear strains is $2\langle\varepsilon_{12}\rangle \approx 15\%$. The comparison between analytical and experimental shear stress-strain curves is in Figure 17. Once again, it is noticeable a good analytical-experimental agreement showing the capacity of the proposed model.
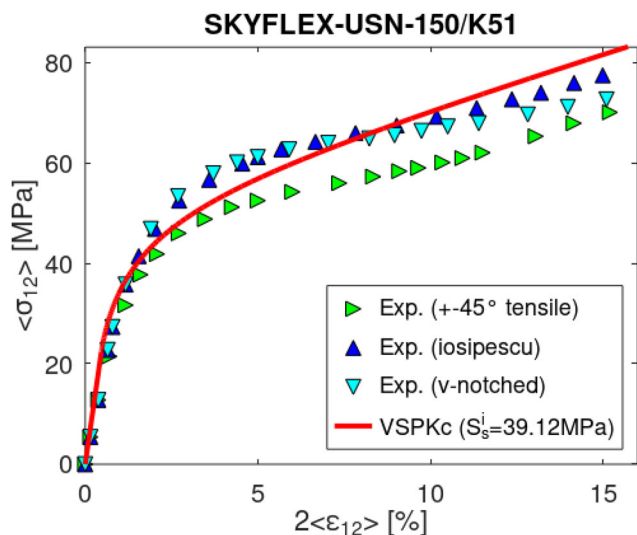
Figure 17. Experimental and VSPKc in-plane shear stress-strain curves using the points with $2\langle\varepsilon_{12}\rangle = 5\%$ and assuming $\lambda = 2$ and $V_i = 0.1$ for SKYFLEX-USN-150/K51 lamina. Experimental data from Choi et al. [59].

7. Conclusions

This paper presents a novel analytical model for in-plane shear response of unidirectional composite with a square unit cell and a finite dimension fiber-matrix interface. The interface is considered assuming three zones: core, fiber-transition and matrix-transition. The effect of this interface on the deformation of composite is analyzed. Elastic properties are evaluated by considering just the core zone interface, changing the composite stiffness. The fiber-transition zone is responsible for material nonlinearity due to interface damage. The proposed approach is based on the VSPKc model to evaluate the load share from micromechanical point of view. Experimental verification is carried out showing the capability of model to describe the phenomena under study. Besides, a comparison with FE simulation shows the physical consistence of the proposed model. In general, the novel analytical model is able to obtain estimations in close agreement with experimental data, showing to be a powerful tool for micromechanical analysis of linear and nonlinear behavior of unidirectional laminae subjected to in-plane shear load.

Disclosure statement

No potential conflict of interest was reported by the author(s).

ORCID

Lucas L. Vignoli 🔸 http://orcid.org/0000-0003-3288-3568
Marcelo A. Savi 🔸 http://orcid.org/0000-0001-5454-5995
Pedro M. C. L. Pacheco 🔸 http://orcid.org/0000-0002-3374-5119
Alexander L. Kalamkarov 🔸 http://orcid.org/0000-0002-9964-5882

References

[1] N. Tolosana, D. Ranz, O. Gracia, J. Cuartero, and A. Miravete, A micromechanical composite approach for finite element crashworthiness simulation, Mech. Adv. Mater. Struct., vol. 23, no. 12, pp. 1430–1436, 2016. DOI: 10.1080/15376494.2015.1091529.

[2] L.L. Vignoli, and M.A. Savi, Multiscale failure analysis of cylindrical composite pressure vessel: a parametric study, Lat. Am. j. solids Struct., vol. 15, no. 11, pp. 1–21, 2018. DOI: 10.1590/1679-78254323.

[3] S. Blanco, H. You, T.W. Kerekes, and G.J. Yun, Cure-induced residual stress buildup and distortions of CFRP laminates with stochastic thermo-chemical and viscoelastic models: experimental verifications, Mech. Adv. Mater. Struct., vol. 29, no. 19, pp. 2740–2756, 2022. DOI: 10.1080/15376494.2021.1877376.

[4] A.S. Kaddour, M.J. Hinton, P.A. Smith, and S. Li, The background to the third world-wide failure exercise, J Compos Mater., vol. 47, no. 20-21, pp. 2417–2426, 2013a. DOI: 10.1177/0021998313499475.

[5] A.S. Kaddour, and M.J. Hinton, Maturity of 3D failure criteria for fibre reinforced composites: comparison between theories and experiments: part B of WWFE-II, J Compos Mater., vol. 47, no. 6-7, pp. 925–966, 2013. DOI: 10.1177/0021998313478710.

[6] P.D. Soden, A.S. Kaddour, and M.J. Hinton, Recommendations for designers and researchers resulting from the world-wide failure exercise, Comp Sci Technol., vol. 64, no. 3-4, pp. 589–604, 2004. DOI: 10.1016/S0266-3538(03)00228-8.

[7] P. Díaz-Montiel, S. Venkataraman, and H. Kim, The effects of plasticity mechanisms on micromechanics of composites with fiber waviness defects under compression, Mech. Adv. Mater. Struct., vol. 29, no. 28, pp. 7503–7518, 2022. DOI: 10.1080/15376494.2021.2001121.

[8] X. Hui, Y. Xu, and Y. Hou, A coupled micro–meso-scale study on the damage mechanism of 2D SiC/SiC ceramic matrix composites, Mech. Adv. Mater. Struct., vol. 28, no. 20, pp. 2083–2095, 2021. DOI: 10.1080/15376494.2020.1717021.

[9] B. Shi, Z. Den, L. Tan, Y. Zhao, and X. Zhang, Micromechanics-based reliability analysis method for laminated composite structures, Mech. Adv. Mater. Struct., vol. 28, no. 20, pp. 2096–2113, 2021. DOI: 10.1080/15376494.2020.1717022.

[10] I.V. Andrianov, J. Awrejcewicz, and V.V. Danishevs'kyy, 2018. Asymptotical Mechanics of Composites - Modelling Composites without FEM, Springer, Switzerland.

[11] L.L. Vignoli, M.A. Savi, P.M.C.L. Pacheco, and A.L. Kalamkarov, Multiscale approach to predict strength of notched composite plates, Compos. Struct., vol. 253, pp. 112827, 2020c. DOI: 10.1016/j.compstruct.2020.112827.

[12] A.L. Kalamkarov, and A.G. Kolpakov, 1997. Analysis, Design and Optimization of Composite Structures, 2nd edition, Wiley, Chichester, NY.

[13] R. Talreja, and A.M. Waas, Concepts and definitions related to mechanical behavior of fiber reinforced composite materials, Compos. Sci. Technol., vol. 217, pp. 109081, 2022. DOI: 10.1016/j.compscitech.2021.109081.

[14] L.L. Vignoli, and J.T.P. Castro, A parametric study of stress concentration issues in unidirectional laminates, Mech. Adv. Mater. Struct., vol. 28, no. 15, pp. 1554–1569, 2021. DOI: 10.1080/15376494.2019.1688434.

[15] Z. Xiong, C. Zhao, Y. Meng, and W. Li, A damage model based on Tsai–Wu criterion and size effect investigation of pultruded GFRP, Mechanics of Advanced Materials and Structures, in Press., pp. 1–15, 2022. DOI: 10.1080/15376494.2022.2116754.

[16] M.A. Caminero, M. Lopez-Pedrosa, C. Pinna, and C. Soutis, Damage monitoring and analysis of composite laminates with

an open hole and adhesively bonded repairs using digital image correlation, Composites: part B., vol. 53, pp. 76–91, 2013. DOI: 10.1016/j.compositesb.2013.04.050.

[17] T. Laux, K.W. Gan, R.P. Tavares, C. Furtado, A. Arteiro, P.P. Camanho, O.T. Thomsen, and J.M. Dulieu-Barton, Modelling damage in multidirectional laminates subjected to multi-axial loading: ply thickness effects and model assessment, Compos. Struct., vol. 266, pp. 113766, 2021. DOI: 10.1016/j.compstruct.2021.113766.

[18] P.P. Kenedi, L.L. Vignoli, B.T. Duarte, J.S.S. Neto, and C.F.C. Bandeira, Damage tracking of notched composite plates by thermography—Experimental observations and analytical model for damage onset, J. Compos. Mater., vol. 56, no. 8, pp. 1211–1220, 2022. DOI: 10.1177/00219983211072297.

[19] L.L. Vignoli, and P.P. Kenedi, Hybrid multiscale procedure for damage in notched unidirectional composite monitored by thermography, Polym. Compos., vol. 43, no. 7, pp. 4288–4296, 2022. DOI: 10.1002/pc.26689.

[20] L.L. Vignoli, P.P. Kenedi, and M.J.B. Mariano, Exploring thermography technique to validate multiscale procedure for notched CFRP plates, Composites Part C: open Access., vol. 7, pp. 100241, 2022b. DOI: 10.1016/j.jcomc.2022.100241.

[21] L.L. Vignoli, R.M.C. Neto, M.A. Savi, P.M.C.L. Pacheco, and A.L. Kalamkarov, Trace theory applied to composite analysis: a comparison with micromechanical models, Compos. Commun., vol. 25, pp. 100715, 2021. DOI: 10.1016/j.coco.2021.100715.

[22] L.L. Vignoli, M.A. Savi, P.M.C.L. Pacheco, and A.L. Kalamkarov, Comparative analysis of micromechanical models for the elastic composite laminae, Composites Part B: engineering., vol. 174, pp. 106961, 2019. DOI: 10.1016/j.compositesb.2019.106961.

[23] L.L. Vignoli, M.A. Savi, P.M.C.L. Pacheco, and A.L. Kalamkarov, A Novel Micromechanical Model Based on the Rule of Mixtures to Estimate Effective Elastic Properties of Circular Fiber Composites, Appl. Compos. Mater., vol. 29, no. 4, pp. 1715–1731, 2022a. DOI: 10.1007/s10443-022-10038-z.

[24] Vignoli, L.L. Savi, M.A. Pacheco, P. M.C.L, and Kalamkarov, A.L., Micromechanical analysis of transversal strength of composite laminae, Compos. Struct., vol. 250, pp. 112546, 2020a. DOI: 10.1016/j.compstruct.2020.112546.

[25] L.L. Vignoli, M.A. Savi, P.M.C.L. Pacheco, and A.L. Kalamkarov, Micromechanical analysis of longitudinal and shear strength of composite laminae, J. Compos. Mater., vol. 54, no. 30, pp. 4853–4873, 2020b. DOI: 10.1177/0021998320936343.

[26] S. Li, M. Xu, S. Yan, and E. Sitnikova, On the objectivity of the nonlinear along-fibre shear stress–strain relationship for unidirectionally fibre-reinforced composites, J. Eng. Math., vol. 127, no. 1, pp. 17, 2021. DOI: 10.1007/s10665-021-10098-3.

[27] C.N. O'Brien, and Arash E. Zaghi, Modelling the nonlinear shear stress-strain response of composites with metal and non-metal reinforcement, Composites Part B., vol. 221, pp. 109009, 2021. DOI: 10.1016/j.compositesb.2021.109009.

[28] A. Sabik, In-plane shear nonlinearity in failure behavior of angle-ply laminated shells, Compos. Struct., vol. 225, pp. 111164, 2019. DOI: 10.1016/j.compstruct.2019.111164.

[29] N.R. Kolanu, G. Raju, and M. Ramji, Damage assessment studies in CFRP composite laminate with cut-out subjected to in-plane shear loading, Composites Part B., vol. 166, pp. 257–271, 2019. DOI: 10.1016/j.compositesb.2018.11.142.

[30] X. Chen, X. Sun, B. Wang, J. Gu, P. Zou, Y. Chai, and J. Yang, An improved longitudinal failure criterion for UD composites based on kinking model, Mech. Adv. Mater. Struct., vol. 29, no. 6, pp. 905–915, 2022. DOI: 10.1080/15376494.2020.1799269.

[31] I.V. Andrianov, V.I. Bolshakov, V.V. Danishevs'kyy, and W. Weichert, Asymptotic simulation of imperfect bonding in periodic fibre-reinforced composite materials under axial shear, Int. J. Mech. Sci., vol. 49, no. 12, pp. 1344–1354, 2007. DOI: 10.1016/j.ijmecsci.2007.04.002.

[32] D. Zhang, and A.M. Waas, A micromechanics based multiscale model for nonlinear composites, Acta Mech., vol. 225, no. 4-5, pp. 1391–1417, 2014. DOI: 10.1007/s00707-013-1057-1.

[33] D.K. Patel, A.D. Hasanyan, and A.M. Waas, N-Layer concentric cylinder model (NCYL): an extended micromechanics-based multiscale model for nonlinear composites, Acta Mech., vol. 228, no. 1, pp. 275–306, 2017. DOI: 10.1007/s00707-016-1696-0.

[34] M. Würkner, H. Berger, and U. Gabbert, Numerical study of effective elastic properties of fiber reinforced composites with rhombic cell arrangements and imperfect interface, Int. J. Eng. Sci., vol. 63, pp. 1–9, 2013. DOI: 10.1016/j.ijengsci.2012.10.002.

[35] I. Sevostianov, R. Rodriguez-Ramos, R. Guinovart-Diaz, J. Bravo-Castillero, and F.J. Sabina, Connections between different models describing imperfect interfaces in periodic fiber-reinforced composites, Int. J. Solids Struct., vol. 49, no. 13, pp. 1518–1525, 2012. DOI: 10.1016/j.ijsolstr.2012.02.028.

[36] L. Riaño, L. Belec, J.F. Chailan, and Y. Joliff, Effect of interphase region on the elastic behavior of unidirectional glass fiber/epoxy composites, Compos. Struct., vol. 198, pp. 109–116, 2018. DOI: 10.1016/j.compstruct.2018.05.039.

[37] S. Subramanian, J.J. Lesko, K.L. Reifsnider, and W.W. Stinchcomb, Characterization of the Fiber-Matrix Interphase and its Influence on Mechanical Properties of Unidirectional Composites, J. Compos. Mater., vol. 30, no. 3, pp. 309–332, 1996. DOI: 10.1177/002199839603000302.

[38] J. Koyanagi, H. Nakatani, and S. Ogihara, Comparison of glass–epoxy interface strengths examined by cruciform specimen and single-fiber pull-out tests under combined stress state, Composites: part A., vol. 43, no. 11, pp. 1819–1827, 2012. DOI: 10.1016/j.compositesa.2012.06.018.

[39] Y. Zhou, and Z.M. Huang, Prediction of In-Plane Shear Properties of a Composite with Debonded Interface, Appl. Compos. Mater., vol. 29, no. 2, pp. 901–935, 2022. DOI: 10.1007/s10443-021-09982-z.

[40] W.G. Jiang, Z.K. Wu, L. Zheng, and Q.H. Qin, A simplified micromechanical model for predicting effective mechanical behaviors of continuous bidirectional-fiber-reinforced composites, Mech. Adv. Mater. Struct., vol. 24, no. 15, pp. 1292–1299, 2017. DOI: 10.1080/15376494.2016.1227505.

[41] Y. Huang, C.A. Cimini, Jr., and S.K. Ha, A micromechanical unit cell model with an octagonal fiber for continuous fiber reinforced composites, J. Compos. Mater., vol. 54, no. 28, pp. 4495–4513, 2020. DOI: 10.1177/0021998320913939.

[42] N. Agwu, and C.G. Ozoegwu, Critical investigation on the effect of fiber geometry and orientation on the effective mechanical properties of fiber-reinforced polymer composites, Mech. Adv. Mater. Struct., vol. 30, no. 15, pp. 3051–3060, 2023. DOI: 10.1080/15376494.2022.2068206.

[43] D.C. Hammerand, G.D. Seidel, and D.C. Lagoudas, Computational Micromechanics of Clustering and Interphase Effects in Carbon Nanotube Composites, Mech. Adv. Mater. Struct., vol. 14, no. 4, pp. 277–294, 2007. DOI: 10.1080/15376490600817370.

[44] K. Wang, Y. Lu, Y. Rao, N. Wei, J. Ban, Y. Peng, S. Yao, and S. Ahzi, New insights into the synergistic influence of voids and interphase characteristics on effective properties of unidirectional composites, Compos. Struct., vol. 255, pp. 112862, 2021. DOI: 10.1016/j.compstruct.2020.112862.

[45] S.K. Ha, K.K. Jin, and Y. Huang, Micro-Mechanics of Failure (MMF) for Continuous Fiber Reinforced Composites, J. Compos. Mater., vol. 42, pp. 1873–1895, 2008.

[46] R.Q. Macedo, R.T.L. Ferreira, J.M. Guedes, and M.V. Donadon, Intraply failure criterion for unidirectional fiber reinforced composites by means of asymptotic homogenization, Compos. Struct., vol. 159, pp. 335–349, 2017. DOI: 10.1016/j.compstruct.2016.08.027.

[47] I.G. García, M. Paggi, and V. Mantic, Fiber-size effects on the onset of fiber–matrix debonding under transverse tension: a comparison between cohesive zone and finite fracture mechanics models, Eng. Fract. Mech., vol. 115, pp. 96–110, 2014. DOI: 10.1016/j.engfracmech.2013.10.014.

[48] Z. Tang, C. Wang, and Y. Yu, Failure response of fiber-epoxy unidirectional laminate under transverse tensile/compressive loading

using finite-volume micromechanics, Composites Part B., vol. 79, pp. 331–341, 2015. DOI: 10.1016/j.compositesb.2015.04.054.

[49] L. Zhuang, A. Pupurs, J. Varna, R. Talreja, and Z. Ayadi, Effects of inter-fiber spacing on fiber-matrix debond crack growth in unidirectional composites under transverse loading, Composites Part A., vol. 109, pp. 463–471, 2018. DOI: 10.1016/j.compositesa.2018.03.031.

[50] J. Zhang, J. Wang, Z. Yuan, and H. Jia, Effect of the cohesive law shape on the modelling of adhesive joints bonded with brittle and ductile adhesives, Int. J. Adhes. Adhes., vol. 85, pp. 37–43, 2018. DOI: 10.1016/j.ijadhadh.2018.05.017.

[51] R.L. Fernandes, and R.D.S.G. Campilho, Accuracy of cohesive laws with different shape for the shear behaviour prediction of bonded joints, The Journal of Adhesion., vol. 95, no. 4, pp. 325–347, 2019. DOI: 10.1080/00218464.2018.1438895.

[52] E.J. Barbero, 2008. Finite Element Analysis of Composite Materials, CRC Press.

[53] A.S. Kaddour, M.J. Hinton, P.A. Smith, and S. Li, Mechanical properties and details of composite laminates for the test cases used in the third world-wide failure exercise, J Compos Mater., vol. 47, no. 20-21, pp. 2427–2442, 2013b. DOI: 10.1177/0021998313499477.

[54] A. Matzenmiller, and S. Gerlach, Parameter identification of elastic interphase properties in fiber composites, Composites: part B., vol. 37, no. 2-3, pp. 117–126, 2005. DOI: 10.1016/j.compositesb.2005.08.003.

[55] A.R. Maligno, N.A. Warrior, and A.C. Long, Effects of interphase material properties in unidirectional fibre reinforced composites, Compos. Sci. Technol., vol. 70, no. 1, pp. 36–44, 2010. DOI: 10.1016/j.compscitech.2009.09.003.

[56] C. Chang, Y. Zhang, and H. Wang, Micromechanical modeling of unidirectional composites with random fiber and interphase thickness distributions, Arch. Appl. Mech., vol. 89, no. 12, pp. 2563–2575, 2019. DOI: 10.1007/s00419-019-01595-0.

[57] X. Wang, J. Zhang, Z. Wang, S. Zhou, and X. Sun, Effects of interphase properties in unidirectional fiber reinforced composite materials, Mater. Des., vol. 32, no. 6, pp. 3486–3492, 2011. DOI: 10.1016/j.matdes.2011.01.029.

[58] ASTM D3518M-18, 2018. Standard Test Method for in-Plane Shear Response of Polymer Matrix Composite Materials by Tensile Test of a ± 45° Laminate, American Society for Testing and Materials - ASTM International, West Conshohocken, PA.

[59] J.H. Choi, J. Jang, W. Shim, J.-M. Cho, S.-J. Yoon, C.-H. Choi, H.N. Han, and W.-R. Yu, Determination of the in-plane shear modulus of unidirectional carbon fiberreinforced plastics using digital image correlation and finite-element analysis, Compos. Struct., vol. 229, pp. 111392, 2019. DOI: 10.1016/j.compstruct.2019.111392.

[60] ASTM D5379M-12, 2012. Standard Test Method for Shear Properties of Composite Materials by the V-Notched Beam Method, American Society for Testing and Materials - ASTM International, West Conshohocken, PA.

[61] ASTM D7078M-12, 2012. Standard Test Method for Shear Properties of Composite Materials by V-Notched Rail Shear Method. American Society for Testing and Materials - ASTM International, West Conshohocken, PA.

[62] ASTM D4762-18, 2018. Standard Guide for Testing Polymer Matrix Composite Materials, American Society for Testing and Materials - ASTM International, West Conshohocken, PA.